Inorganica Chimica Acta 407 (2013) 306–312

Contents lists available at ScienceDirect

Inorganica Chimica Acta

journal homepage: www.elsevier.com/locate/ica

Preparation, crystallographic and theoretical study on a bifunctional Gd-AAZTA derivative as potential MRI contrast agent precursor

R. Artali [a], G. Bombieri [a], G.B. Giovenzana [b], M. Galli [c], L. Lattuada [c], F. Meneghetti [a,*]

[a] Dipartimento di Scienze Farmaceutiche, Università degli Studi di Milano, Via L. Mangiagalli 25, 20133 Milano, Italy
[b] Dipartimento di Scienze del Farmaco, Università degli Studi del Piemonte Orientale "A. Avogadro", Largo Donegani 2/3, 28100 Novara, Italy
[c] Centro Ricerche Bracco, Bracco Imaging Spa, Via Ribes 5, 10010 Colleretto Giacosa (TO), Italy

ARTICLE INFO

Article history:
Received 12 June 2013
Received in revised form 2 August 2013
Accepted 2 August 2013
Available online 17 August 2013

Keywords:
AAZTA derivative
Gd(III) complex
MRI contrast agent
Crystal structure

ABSTRACT

The crystal structure of the complex (αR,6R)-Na[Gd(H_2O)-AAZTA-C_2H_4COOBn]·3H_2O·EtOH was determined by single crystal X-ray diffraction; the complex represents a bifunctional derivative of Gd-AAZTA, previously reported as original scaffold for the development of efficient contrast agents for MRI. The Gd(III) ion is nine coordinated with three nitrogens, five carboxylate oxygens and one water oxygen in a monocapped distorted square antiprism coordination polyhedron. Three of the five carboxylic groups are monodentate while a fourth is bidentate bridging an adjacent Gd ion with the formation of a polymeric structure. The influence on the overall structure of the propionate side arm introduced for conjugation purposes was discussed, and a computational approach to predict the structure of its (αR,6S) isomer is presented and compared with the X-ray structure of the (αR,6R) epimer.

1. Introduction

Lanthanide complexes are used in several areas of chemistry, biology and medicine, due to their wide variety of optical, magnetic and radiochemical properties. The favourable electronic relaxation of paramagnetic Gd(III) makes this element the most used lanthanide ion for clinical application in MRI examinations. Nowadays, MRI represents one of the most important diagnostic technique in medicine, based primarily on the use of paramagnetic Gd(III) complexes as CAs (Contrast Agent) and more than 30 millions clinical scans are annually performed. An improvement of the image, meaning better contrast enhancement between healthy and diseased tissue and organs, is the goal of MRI CAs. In this respect, the administration of a paramagnetic complex causes a remarkable change of relaxivity of the tissue water protons when exposed to an external magnetic field. Nevertheless, one of the major problems met with this technique is to avoid the release of toxic Gd(III) aquoions for *in vivo* applications [1,2]. This requires the use of highly stable complexes from both the thermodynamic and kinetic point of view, usually relying on octadentate polyaminopolycarboxylic ligands. The two archetypal Gd(III)-based CAs employed are the complexes with the well known linear ligand DTPA (DTPA = diethylenetriaminopentacetic acid) and the macrocyclic ligand DOTA (DOTA = 1,4,7,10-tetraazacyclododecane-1,4,7,10-tetraacetic acid). Nowadays other Gd(III) complexes are currently employed in the clinical practice and their structure is generally based on DTPA or DOTA ligands, bearing different substituents mainly devoted to the modification of the biodistribution [1,2]. Acyclic ligands are cheaper, but their complexes present lower thermodynamic and kinetic stabilities; slow complex dissociation from complexes with some acyclic ligands was recently observed in patients with renal failure leading to specific pathologies such as NSF [3]. On the other hand, outstanding stabilities are observed with macrocyclic ligands, with Gd–DOTA complexes having half-lives in 0.1 M HCl more than five orders of magnitude higher than those of Gd–DTPA bis-amides [4,5] and associated to a safer *in vivo* use.

The efficiency of a Gd(III) chelate as MRI CA is measured mainly as relaxivity (the increase in the relaxation rate of the observed nucleus for a 1 mM concentration of the CA) that essentially relies on the number of water molecules in the inner coordination sphere of the paramagnetic metal ("*q*" term), although the increase of the latter parameter contrasts with the necessity of having high denticity ligands for higher stability. Relaxivity values in water of 4–5 mM^{-1} s^{-1} are consistent with small sized Gd(III) CAs, with one water molecule coordinated to the metal. The search for stable Gd(III) chelates with more than one water molecule in the inner metal coordination sphere is in continuous progress, as witnessed by the hydroxy-pyridinone based structures (HOPOs) developed by Raymond and coworkers [6–8] and the *N*-alkyldiethylenetriamine-tetraacetic acid derivatives reported by Caravan [9] and Merbach [10].

* Corresponding author. Tel.: +39 0250319306.
E-mail address: fiorella.meneghetti@unimi.it (F. Meneghetti).

0020-1693/$ - see front matter © 2013 Elsevier B.V. All rights reserved.
http://dx.doi.org/10.1016/j.ica.2013.08.004

More recently the AAZTA derivatives (AAZTA = 1,4-bis(carboxymethyl)-6-[bis(carboxymethyl)]-amino-6-methyl-1,4-diazepane) [11] were proposed, showing a good compromise between higher metal hydration and a good thermodynamic and an excellent kinetic stability [12]. The AAZTA ligand is formed by a seven-membered ring with two endocyclic and one exocyclic nitrogen atoms and four carboxymethyl side arms, representing a novel intermediate family between the open chain DTPA and macrocyclic DOTA ligands. Its Gd(III) complex, Gd-AAZTA^{-}, presents a relaxivity 65–70% higher than Gd–DTPA^{2-} and Gd–DOTA^{-}, ensured by the two coordinated water molecules.

The crystal structure determinations of the ligand AAZTA and of the corresponding Gd(III) complex Na[Gd-AAZTA(H_2O)]·3H_2O show for the ligand a zwitterion with two deprotonated carboxylic groups and two protonated tertiary nitrogen atoms [13], while the gadolinium complex is a centrosymmetric dimer with a bicapped square antiprismatic geometry and an inner sphere water for each half of the dimer.

A lipophylic derivative with a longer aliphatic chain [14] showed a strong non-covalent interaction with human serum albumin, boosting the relaxivity to a value of about 80 mM^{-1} s^{-1}, the highest value reported to date for this class of CA; moreover, this lipophilic Gd-AAZTA derivative was used to form non-covalent conjugates with HDL [15] and LDL [16], taking advantage of the uptake of labelled lipoproteins by tumor cells for their better visualization. Additional derivatives of the parent ligand include: (i) an additional lipophilic double-chain AAZTA, successfully employed to label cells on their outer surface [17], (ii) bifunctional derivatives useful for conjugation to vectors [18,19], (iii) oligomers such as a dimer [20], where the relaxivity is more than doubled than that of the monomeric Gd-AAZTA in virtue of a significant contribution arising from the increased molecular reorientational time and from water molecules in the second coordination sphere of the Gd(III) ions, and multimers where up to 8 Gd-AAZTA units were linked to a central PAMAM dendrimeric scaffold [21].

The growing list of application of Gd-AAZTA to MRI studies prompted our research towards bifunctional derivatives of AAZTA, where a reactive functional group is introduced on the ligand structure, allowing the conjugation of the AAZTA or of the corresponding complexes to desired "vectors" [22]. Most of the reported bifunctional derivatives of AAZTA bear the functional group in the position 6 of the 1,4-diazepane ring, due to their synthetic accessibility and because this choice places the conjugation site remote to the metal coordination sphere. Recently we reported a synthetic access to alternative bifunctional AAZTA derivatives, embodying a functionalized side chain placed on the α-position of the carboxymethyl side arms [23]. This strategy allows to leave unaltered the diazepane ring and gives access to a large variety of bifunctional derivatives; nevertheless, the close proximity of the functional substituents to the metal coordination sphere could have an adverse effect on the exchange rate of the water molecule(s) coordinated to the metal center.

Here we report a crystallographic and computational study on the AAZTA derivative Gd(H_2O)-**L** (**L** = AAZTA-C_2H_4COOBn *i.e.* bis(carboxymethyl)amino]-α-[3-(phenylmethoxy)-3-oxopropyl]-6-methyl-1,4-diazepane-1,4-diacetate, Chart 1), with the aim of defining the possible influence of steric hindrance on the water exchange rate of its two diastereoisomers (α*R*,6*R*)-Gd(H_2O)-**L** (**1**) and (α*R*,6*S*)-Gd(H_2O)-**L** (**2**).

Suitable crystals for X-ray diffraction analysis were obtained only for the (α*R*,6*R*) diastereoisomer (**1**). A computational approach to predict the structure of the (α*R*,6*S*)-Gd(H_2O)-**L** (**2**) diastereoisomer is presented and compared with the X-ray structure of its epimer (α*R*,6*R*) (**1**). The models of both diastereoisomers were analyzed by molecular dynamics simulations in explicit solvent environment (water).

The results obtained could be useful in evaluating the features of these novel MRI contrast agents and the effect on the exchange of water molecules coordinated to the paramagnetic metal ion.

2. Experimental

2.1. Instrumentation

The ^{1}H and ^{13}C spectra were recorded on a Bruker Avance 400 instrument. Mass spectra were recorded with a ThermoFinnigan TSQ700 triple-quadrupole instrument equipped with an electrospray ionization source. HPLC was performed on a Merck-Hitachi L6200 and L6000 system equipped with an AS2000 autosampler, a T6300 column thermostat and a L4250 UV detector (210 nm). HPLC method: stationary phase: Lichrospher 60 RP-Select B 5 μm, 75 × 4 mm column packed by Merck KGaA and thermostated at 45 °C; mobile phase: eluent *A* = 0.01 M KH_2PO_4 and 0.017 M H_3PO_4 in H_2O, eluent B = MeCN; gradient elution: *t* = 0 min (5% B), *t* = 15 min (80% B), *t* = 20 min (80% B). Capillary electrophoresis (CE) was performed on a Hewlett Packard 3D CE instrument. CE method: stationary phase: fused silica, 56 cm × 50 μm (i.d.), buffer: 50 mM borate and 0.3 mM EDTA (pH 9.3), UV detection (200 nm).

2.2. Materials

Reagent-grade chemicals were obtained from commercial sources and used without further purification. The synthesis of 6-methyl-1,4-diazepane-6-amine **3** [11] and (2*S*)-2-bromopentanedioic acid 1-(1,1-dimethylethyl)-5-(phenylmethyl) ester **4** [24] were performed as reported in the literature.

2.3. Synthesis of (αR)-6-amino-6-methyl–[3-oxo-3-(phenylmethoxy)propyl]-1,4-diazepane-1,4-acetic acid (1,1-dimethylethyl) ester 5 (diastereoisomers mixture)

A suspension of 6-methyl-1,4-diazepane-6-amine **3** (6.62 g; 51.3 mmol) and K_2CO_3 (2.13 g; 15.4 mmol) in MeCN (130 mL) was cooled to 0 °C. A solution of (2*S*)-2-bromopentanedioic acid 1-(1,1-dimethylethyl)-5-(phenylmethyl) ester **4** (5.5 g; 15.4 mmol) in MeCN (30 mL) was dropped into the suspension in 35 min. After this time, the mixture was allowed to warm to room temperature and stirred for 4 h. The mixture was filtered and the solution evaporated at reduced pressure. The crude residue was dissolved in EtOAc (150 mL) and washed with water (3 × 100 mL) to eliminate unreacted **3**. The organic phase was extracted with 0.01 M HBr (3 × 100 mL). The aqueous phase was brought to pH 9 with 25% NH_4OH, then extracted with EtOAc (4 × 70 mL). The combined organic phases were washed with water (100 mL), dried over Na_2SO_4 and evaporated to give **5** as a mixture of diastereoisomers (Major : minor = 63 : 37). Yield: 4.81 g, 77%. HPLC: 99.1% (Area%). ^{1}H NMR (400 MHz, $CDCl_3$) δ: 7.36–7.29 ($5H^M + 5H^m$, m), 5.123 ($2H^m$, s), 5.116 ($2H^M$, s), 3.19 ($1H^m$, dd, *J* = 9.6, 5.9 Hz), 3.16 ($1H^M$, dd, *J* = 9.0, 6.2 Hz), 2.94–2.45 ($10H^M + 10H^m$, m), 2.08–1.98 ($1H^M + 1H^m$, m), 1.95–1.82 ($1H^M + 1H^m$, m), 1.64 ($3H^M + 3H^m$, bs), 1.45 ($9H^M + 9H^m$, s), 0.96 ($3H^M$, s), 0.95 ($3H^m$, s) ppm. ^{13}C NMR ($CDCl_3$) δ: 173.50 (C^M), 173.49 (C^m), 172.10 (C^M), 172.03 (C^m), 136.3 ($C^M + C^m$), 128.9 ($CH^M + CH^m$), 128.68–128.63 ($2CH^M + 2CH^m$), 81.5 ($C^M + C^m$), 69.4 ($CH_2{}^m$), 69.1 ($CH_2{}^M$), 68.9 ($CH_2{}^m$), 67.4 ($CH_2{}^M$), 66.69 ($CH_2{}^m$), 66.67 ($CH_2{}^M$), 63.2 ($CH_2{}^M$), 62.7 ($CH_2{}^m$), 56.0 ($CH_2{}^M$), 54.1 ($CH_2{}^m$), 53.8 (C^M), 53.6 (C^m), 52.4 ($CH_2{}^M$), 51.8 ($CH_2{}^m$), 31.5 ($CH_2{}^m$), 31.4 ($CH_2{}^M$), 28.7 ($CH_3{}^M + CH_3{}^m$), 26.8 ($CH_3{}^M$), 26.4 ($CH_3{}^m$), 25.9 ($CH_2{}^M$), 25.8 ($CH_2{}^m$) ppm. ESI-MS *m*/*z* ($C_{22}H_{35}N_3O_4$, calc.: 405.3): 428.5 (MNa^+), 406.4 (MH^+), 350.3 (MH^+-*t*Bu).

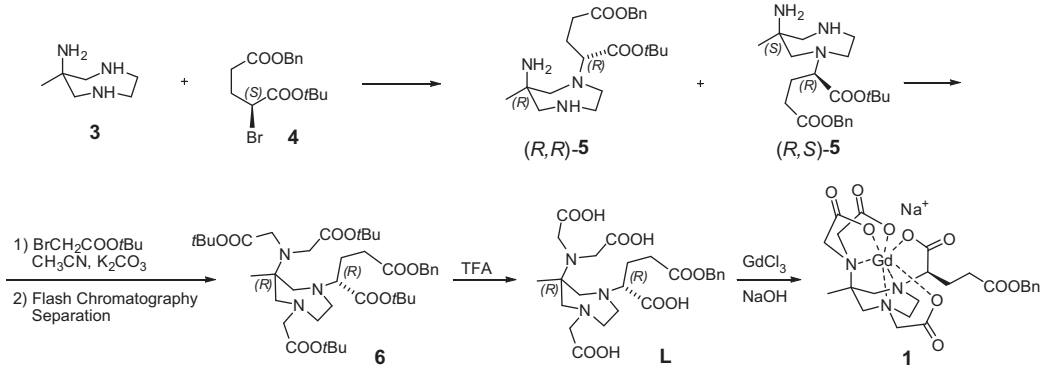

Chart 1. Synthetic scheme.

2.4. Synthesis of (αR,6R)-6-[bis[2-(1,1-dimethylethoxy)-2-oxoethyl]amino]-6-methyl–[3-oxo-3-(phenylmethoxy)propyl]-1,4-diazepane-1,4-diacetic acid, bis(1,1-dimethylethyl) ester, **6**

tert-Butyl bromoacetate (7.86 g, 40.3 mmol) was added to a suspension of **5** (4.65 g, 11.5 mmol), crushed K_2CO_3 (6.36 g, 46 mmol) and Na_2SO_4 (1.5 g, 10.6 mmol) in MeCN (80 mL). The mixture was heated at reflux and stirred for 16 h. The mixture was filtered and evaporated at reduced pressure to give a crude which was purified by flash chromatography (silica gel, eluent: 1:9 EtOAc/petroleum ether) giving the single diastereoisomer **6** (0.6 g) and a mixture of diastereoisomers (6.66 g). Yield: 0.6 g, 7%. HPLC: 92% (Area%). ^{1}H NMR ($CDCl_3$) δ: 7.37–7.31 (5H, m), 5.13 (2H, s), 3.71 (2H, d, J = 7.8 Hz), 3.67 (2H, d, J = 17.8 Hz), 3.34 (1H, d, J = 16.9 Hz), 3.28 (1H, d, J = 16.9 Hz), 3.15 (1H, dd, J = 10.0, 5.7 Hz), 3.07 (1H, d, J = 11.0 Hz), 3.04 (1H, d, J = 11.4 Hz), 2.77 (1H, d, J = 10.8 Hz), 2.60 (1H, d, J = 10.8 Hz), 2.74–2.55 (4H, m), 2.53–2.48 (2H, m), 2.05–1.96 (1H, m), 1.91–1.75 (1H, m), 1.46 (9H, s), 1.45 (9H, s), 1.43 (18H, s), 1.01 (3H, s) ppm. ^{13}C NMR ($CDCl_3$) δ: 173.6 (C), 173.0 (C), 172.2 (C), 171.4 (C), 136.4 (C), 128.9 (CH), 128.7 (CH), 128.6 (CH), 81.4 (C), 81.1 (C), 80.6 (C), 69.5 (CH), 67.5 (CH_2), 66.8 (CH_2), 66.7 (CH_2), 62.2 (CH_2), 61.4 (C), 60.2 (CH_2), 52.7 (CH_2), 52.0 (CH_2), 31.3 (CH_2), 28.8 (CH_3), 28.6 (CH_3), 28.5 (CH_3), 25.3 (CH_2), 24.5 (CH_3) ppm. ESI-MS m/z ($C_{40}H_{65}N_3O_{10}$, calc.: 747.5): 770.6 (MNa^+), 748.5 (MH^+), 714.5 (MNa^+-tBu), 692.4 (MH^+-tBu).

2.5. Synthesis of (αR,6R)-6-[bis(carboxymethyl)amino]-6-methyl–[3-oxo-3-(phenylmethoxy)propyl]-1,4-diazepane-1,4-diacetic acid, (**L**) and preparation of (αR,6R)-[6-[Bis[(carboxy-κO)methyl]amino-κN]-6-methyl–[3-oxo-3-(phenylmethoxy)propyl]-1,4-diazepane-1,4-diacetato(4-)-κN1,κN4,κO1,κO4]-gadolinate(1-) sodium (**1**)

Compound **6** (472 mg, 0.63 mmol) was cooled at 0 °C then TFA (5 mL) was added. After 20 min the solution was allowed to warm to room temperature and stirred for one night. The solution was evaporated and the residue was taken up with CH_2Cl_2 (5 mL) and the solution evaporated. This operation was repeated four times. The oily residue was treated with Et_2O (4 mL) to obtain a white solid which was separated and dried at the vacuum pump to afford **L**. Yield: 365 mg, 67%. HPLC: 81% (Area %). CE: 86% (Area %). Ligand **L** was directly used in the complexation step.

Ligand **L** (260 mg, 0.5 mmol) was dissolved in water (10 mL) and the pH was adjusted to 5 with 1 M NaOH. This solution was titrated with a 0.025 M aqueous solution of $GdCl_3$ while keeping the pH neutral by addition of 1 M NaOH. The progress of the complexation was monitored by capillary electrophoresis (CE, migration times; t_L = 7.69 min, t_1 = 4.14 min) and by titration of samples of the reaction mixture with 0.001 M aqueous solution of $GdCl_3$ (indicator Xylenol Orange). The solution was desalted by elution on an Amberlite® XAD 16.00 column (35 mL, eluents: H_2O; H_2O/MeCN 9:1, 8:2, 1:1). The fractions collected (15 mL each) were checked by CE and those containing the complex with a purity greater than 90% were pooled and evaporated to give **1** as a white solid. Yield: 42 mg, 12%. CE: 92.2% (Area %). MS (ESI): M+Na^+ at m/z 723.0, 2 M^++Na^+ at m/z 1421.0.

2.6. X-ray analysis

After several attempts, prismatic crystals of the (αR,6R)-Na[Gd(H_2O)-L]·3H_2O·EtOH were obtained by slow evaporation of water/ethanol solutions. Suitable single crystals were used for data collection on an Enraf Nonius CAD4 diffractometer using MoKα radiation. The lattice parameters were determined and refined by least-squares fit of 25 high angle reflections. The structure was solved by direct methods [25] and conventional Fourier synthesis. The refinement by full matrix least-squares [26] on F^2 was anisotropic only for gadolinium and sodium atoms and isotropic for the other non hydrogen atoms due to the scarcely diffracting crystals. The H-atoms positions, were introduced in calculated positions in their described geometries and allowed to ride on the attached carbon atom with fixed isotropic thermal parameters (1.2 U_{eq} of the parent carbon atom) except for the water hydrogens not detected. An ethanol molecule present in the structure was refined isotropically.

Crystallographic and refinement data for the structure are presented in Table 1. Selected bond lengths and angles are reported in Table 2.

The supplementary crystallographic data have been deposited with the Cambridge Crystallographic Data Centre (CCDC deposition number 758026). Copies can be obtained, free of charge, from CCDC, 12 Union Road, Cambridge CB2 1EZ, UK; fax: +44 (1223) 336033; e-mail: deposit@ccdc.cam.ac.uk.

2.7. Molecular modeling

Molecular geometries of the (αR,6R) and (αR,6S) Gd-**L** diastereoisomers calculated at the HF/3-21G [27] level were used in the re-parameterization procedure and as starting geometries in MD simulations; both diastereoisomers were built from the crystallographic structure of (**1**).

Ab initio calculations use the quasi-relativistic effective core potential (ECP) of Dolg et al. [28], (including 46 + 4f^n electrons in the core, leaving the outermost 11 electrons to be treated explicitly), and the [5s4p3d]-GTO valence basis sets for the gadolinium ion. Geometry optimization was performed at the restricted HF level using the 3-21G basis set for the ligand atoms. Solvent effects were

Table 1
Crystal data and structure refinement for (αR,6R)-Na[Gd(H_2O)-**L**]·3H_2O·EtOH.

Empirical formula	$C_{26}H_{43}GdN_3NaO_{15}$
Formula weight	817.8
T (K)	293(2)
λ (Å)	0.71073
Crystal system	orthorhombic
Space group	$P2_12_12_1$
Unit cell dimension, (Å, °)	
a	8.994(2)
b	9.838(5)
c	34.815(8)
V (Å^3)	3080.5(2)
Z	4
D_{calc} (Mg/m^3)	1.744
Absorption coefficient (mm^{-1})	2.232
F (000)	1624
Crystal size (mm)	0.21x0.10x0.08
θ Range (°)	2.15–19.97
Limiting indices	$-1 \leqslant h \leqslant 8$
	$-1 \leqslant k \leqslant 9$
	$-1 \leqslant l \leqslant 33$
Reflections collected/unique	2337/2134
Completeness to θ	99.9%
Refinement method	Full-matrix least-squares on F^2
Data/restraints/parameter	2134/2/199
Goodness-of-fit (GOF) on F^2	1.019
Final R indices [$I > 2\sigma(I)$]	$R_1 = 0.0608$
	$wR_2 = 0.1469$
R indices (all data)	$R_1 = 0.1844$
	$wR_2 = 0.1954$
Largest difference peak and hole (Å^{-3})	0.796 and −0.966

Table 2
Selected bond lengths [Å] and angles [°] of (αR,6R)-Na[Gd(H_2O)-**L**]·3H_2O·EtOH.

Bond lengths		Angles	
Gd–N(1)	2.64(3)	N(3)–Gd–O(1)	94.4(8)
Gd–N(2)	2.56(3)	N(3)–Gd–O(2)	63.6(7)
Gd–N(3)	2.72(2)	N(3)–Gd–O(3)	80.3(8)
Gd–O(1)	2.44(2)	N(3)–Gd–O(4)	131.2(8)
Gd–O(2)	2.37(2)	N(3)–Gd–O(5)	126.0(7)
Gd–O(3)	2.34(2)	N(3)–Gd–O(2)	64.0(8)
Gd–O(4)	2.48(2)	N(3)–Gd–O(9)^{I}	146.1(8)
Gd–O(5)	2.40(2)	O(1)–Gd–O(2)	73.7(9)
Gd–O(2)	2.35(2)	O(1)–Gd–O(3)	143 (1)
Gd–O9^{I}	2.37(2)	O(1)–Gd–O(4)	131.8(7)
		O(1)–Gd–O(5)	73.1(9)
N(1)–Gd–O(1)	141.7(9)	O(1)–Gd–O(2)	73.0(9)
N(1)–Gd–O(2)	121.2(8)	O(1)–Gd–O(9)^{I}	77.2(7)
N(1)–Gd–O(3)	69.2(9)	O(2)–Gd–O(3)	71.7(9)
N(1)–Gd–O(4)	65.5(8)	O(2)–Gd–O(4)	134.9(8)
N(1)–Gd–O(5)	90.0(8)	O(2)–Gd–O(5)	146.0(8)
N(1)–Gd–O(2)	121.6(9)	O(2)–Gd–O(9)^{I}	82.5(8)
N(1)–Gd–O(9)^{I}	135.8(8)	O(3)–Gd–O(4)	70.7(8)
N(1)–Gd–N(2)	69.4(8)	O(3)–Gd–O(5)	138.2(8)
N(1)–Gd–N(3)	67.9(9)	O(3)–Gd–O(9)^{I}	87.3(7)
N(2)–Gd–O(1)	72.4(9)	O(4)–Gd–O(5)	67.7(8)
N(2)–Gd–O(2)	110.6(8)	O(4)–Gd–O(9)^{I}	71.7(7)
N(2)–Gd–O(3)	131.3(8)	O(5)–Gd–O(9)^{I}	83.4(8)
N(2)–Gd–O(4)	112.7(8)		
N(2)–Gd–O(5)	65.2(7)		
N(2)–Gd–O(2)	110.5(9)		
N(2)–Gd–O(9)^{I}	141.2(8)		
N(2)–Gd–N(3)	61.0(8)		

^{I} At $1-x; y-½; ½-z$.

evaluated by GAUSSIAN 03 [29] implementation of the PCM, using the C-PCM variant [30].

The molecular dynamic simulations of the diastereoisomers in aqueous solutions were performed by placing each complex in a periodic cubic box (edge length approximately 3 nm), filled with about 2000 extended simple point charge (SPC/E) water molecules [31]. The simulations were performed by the NAMD package [32], using a modified set of parameters. The non-bonding interactions were evaluated using a twin range cut-off, and the pair list within the shorter-range cut-off (9.0 Å) was evaluated at each step, whereas the pair list within the longer cut-off (14.0 Å) was updated every five steps. A reaction field correction of 78.0 was used to correct for the neglect of electrostatic interactions beyond the 14.0 Å cut-off. The systems were submitted to MD runs at constant temperature and pressure, using the Berendsen algorithm [33]. Complexes and solvent were independently coupled to a temperature bath (298 K) with a coupling time of 0.1 ps, while the pressure was held at 1 bar, with a coupling time of 0.5 ps. The bond lengths of the complexes were constrained using the LINCS algorithm [34], while bond lengths and angles in the water molecules were constrained using the SETTLE algorithm [35]. Time step was 1.0 fs, for a simulation time of 5.0 ns with an equilibration time of 0.1 ns.

3. Results and discussion

3.1. Crystal Structure of the (αR,6R) diastereoisomer (*1*)

In Fig. 1, the asymmetric unit of the complex (αR,6R)-Na[Gd(H_2O)-**L**]·3H_2O EtOH is represented.

The Gd(III) ion is nine coordinated with three nitrogens N(1), N(2), N(3), five carboxylate oxygens O(2), O(3), O(4), O(5), O(9)^{I} (^{I} at $1-x, y-1/2, 1/2-z$) and one water oxygen O(1) in a mono-capped distorted square antiprism coordination polyhedron with the carboxylic oxygen O(4), in axial position (Fig. 2).

One square plane of the antiprism is formed by a carboxylic oxygen O(2), two nitrogens N(2), N(3) and the water oxygen O(1), the other by three carboxyl oxygens O(3), O(5), O(9)^{I} and one nitrogen N(1). The twist angle between the two planes is about 40°. Three of the five carboxylic groups behave as monodentate on the Gd ion, while a fourth bridges an adjacent Gd *via* O(9)^{I}. The insertion of this oxygen in the coordination position is enhanced by the wide angles O(1)–Gd–O(3) and O(1)–Gd–O(4) of 143(1)° and 132(1)°, respectively, responsible also for the short Gd–O(9)^{I} bond distance of 2.39(2) Å with the formation of the polymeric structure illustrated in Fig. 3. The molecular packing clearly indicates the formation of molecular chains developing along the *b* axis, where the hydrophobic parts are facing each other and the position of the water molecules is inside the chains. The eight coordinate sodium ion is embedded deep within the ligand and the crystallized waters of the bulk.

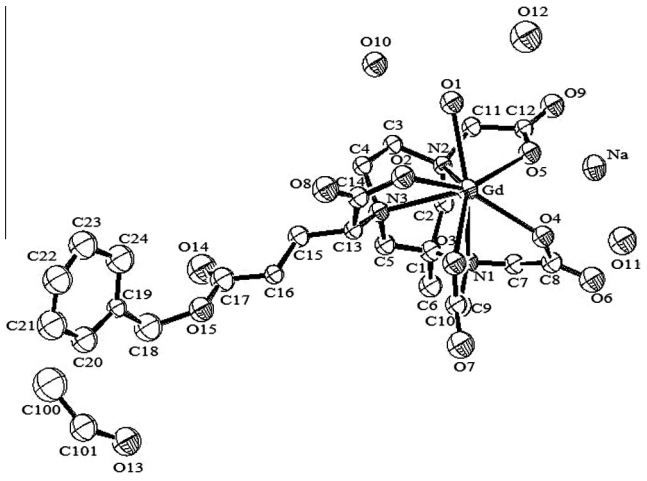

Fig. 1. ORTEP [36] view of (αR,6R)-Na[Gd(H_2O)-**L**]·3H_2O·EtOH with the relative atom-numbering scheme (thermal ellipsoids at 30% probability, hydrogen atoms were omitted for the sake of clarity).

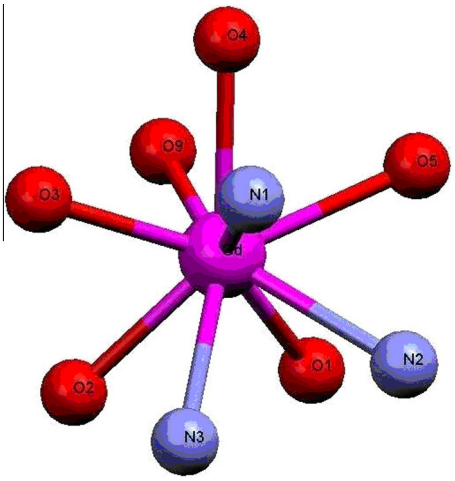

Fig. 2. Ball and stick representation of the coordination polyhedron of (αR,6R)-Na[Gd(H_2O)-**L**]·3H_2O·EtOH including the bridging O9^{I} (^{I} at $1-x;y-½;½-z$).

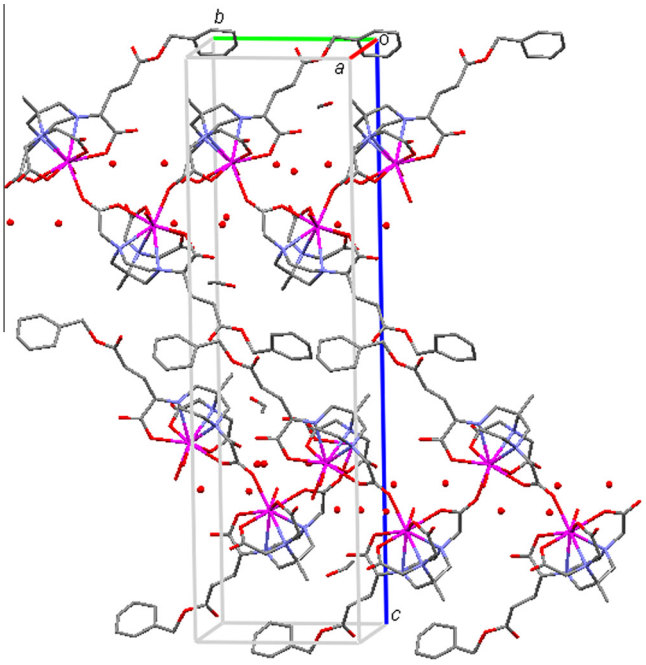

Fig. 3. Crystal packing of (αR,6R)-Na[Gd(H_2O)-**L**]·3H_2O·EtOH showing the molecular chains developing in the *b* axis direction (counterions and hydrogens were omitted for clarity).

The Gd–oxygen bond lengths are rather similar in the limit of their e.s.d.s even though the carboxylic oxygen O(4) in capping position is somewhat larger with a value of 2.48(2) Å, with respect to the average of 2.37(2) Å for the coordinated carboxylic oxygens (Table 2). The Gd–O water distance of 2.44(2) Å, comparable to the value of 2.443(5) Å of Gd-AAZTA [13], is in the range observed for gadolinium monoaquo derivatives (2.45–2.50 Å) [1,37]. Concerning the Gd–N bond distances, it is worthwhile noticing that the largest Gd–N(3) bond (2.72(2) Å) belongs to the heterocyclic nitrogen on the side of the benzyl moiety that could create a kind of tension due to its steric hindrance.

The crystal structure contains, beside the gadolinium coordinated water, three additional water molecules and an ethanol molecule coming from the crystallization solvent.

The close proximity of O(1) to the O(11) and O(12) water molecules is indicative of hydrogen bonds as well the short contacts between the non coordinate waters and the carboxylic oxygens, as reported in details in Table 3.

The addition in AAZTA of an extra moiety C_2H_4COOBn, introduces a stereocenter (*i.e.* C(13)), giving an additional carboxylic group with another potential coordination position, but the hindrance of the attached benzyl moiety disfavours metal coordination and, differently from AAZTA [13], also the possibility of dimeric structures.

The network of hydrogen bonds is related to the presence of four water molecules of which only one metal coordinated is influenced by the extra moiety. In fact, the rather lipophilic substituent creates a kind of belt protecting the polymeric chains on one side and on the other forming lipophilic channels in the structure. The water molecules are interstitially located in the polymeric chains, while in the AAZTA complex [13] they connected the dimer moieties in a 3D network.

3.2. Theoretical investigation

The (αR,6R)-**L**-Gd complex (**1**) was submitted to molecular dynamic calculations starting with two different coordination numbers: the first having the Gd(III) ion octa-coordinated with a water molecule in the first coordination sphere, the second with the metal ion nona-coordinated having two water molecules in the first coordination sphere (the second water molecule occupies the position of the oxygen that allows polymerization in solid state). Fig. 4 shows the conformations for the first and second calculated complexes coloured green and purple respectively, that are superimposed also with the crystal structure.

The results indicate a high overall correspondence in the coordination polyhedron between the predicted models and the X-ray structure but there is no match between the pendant lateral chains. In the X-ray structure, the chain corresponds to the part of the molecule involved in hydrophobic contacts in the crystal packing, which are not present in the molecular dynamics simulation. The sample starting with two coordinated water molecules (purple) exhibits a structure quite perfectly superimposable on the other simulation (green).

The (αR,6S)-**L**-Gd diastereoisomer (**2**) was initially submitted to free dynamic simulation without water molecules coordinated (formally seven coordinated Gd(III) ion), then in the presence of one water coordinated (formally eight coordinated Gd(III) ion). The obtained conformations are represented in blue and light blue respectively, in Fig. 5.

Even in this case, the seven coordinated polyhedron becomes eight coordinated during the simulation process adding a coordinated water molecule, while the second maintains its eight coordination. However, in this latter we notice a poor correspondence for the atom positions in the octacoordinated polyhedrons, differently from that found for the nona-coordinated ones of the diastereoisomer previously analyzed.

The MD calculations started taking into account both diastereoisomers with one water coordinated has revealed a tighter

Table 3
Short contacts (Å) between the waters and the carboxylic oxygens of **L**.

O(1)···O(10)	2.67(4)
O(1)···O(12)	2.75(4)
O(3)···O(12)^{I}	2.82(4)
O(6)···O(10)^{II}	2.75(3)
O(6)···O(11)^{III}	2.66(4)
O(7)···O(10)^{IV}	2.79(3)

^{I} At $1-x;y-½;½-z$.
^{II} At $1-x;y+½;½-z$.
^{III} At $2-x;y+½,½-z$.
^{IV} At $x+1;y;z$.

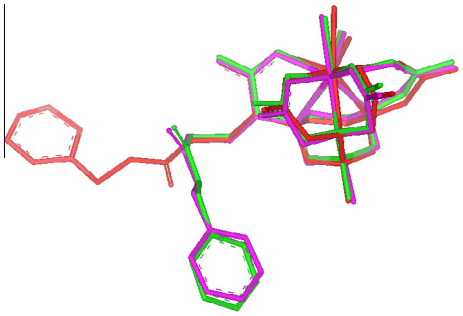

Fig. 4. Overlay of the calculated conformations of (αR,6R)-**L**-Gd diastereoisomer (**1**) (green and purple) onto its crystallographic structure (red) obtained through rms fitting of the heavy atoms. Hydrogen atoms are omitted for the sake of clarity. (For interpretation of the references to colour in this figure legend, the reader is referred to the web version of this article.)

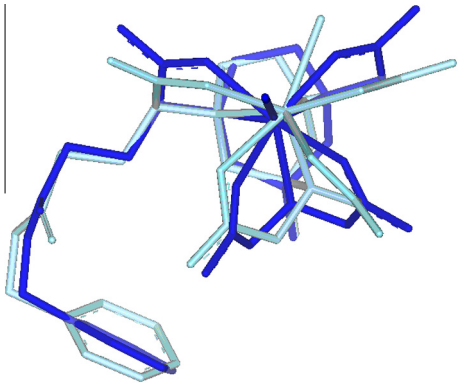

Fig. 5. Superimposition of the calculated structures of diastereoisomer (αR,6S)-**L**-Gd (**2**) obtained through rms fitting of the heavy atoms. Hydrogen atoms are omitted for the sake of clarity.

coordination core surrounding the gadolinium ion for (αR,6S)-**L**-Gd (**2**) with respect to (αR,6R)-**L**-Gd (**1**). This is shown in Fig. 6 where the two resulting conformations are compared and represented in green (**1**) and light blue (**2**).

In particular, we found significant shifts in the respective positions of O5 and O1 and O2, (atom labeling derived from the crystal structure, Fig. 1) that is 2.85 and 4.23 Å apart in the green model and 2.35 and 3.76 Å in the light blue model, respectively. The larger deviations observed in the apical parts of the coordination polyhedron (O5 and O2) are related to the more favourable Van der Waals interactions with the lateral chain, pushing to a more globular and compact structure in the (αR,6S)-**L**-Gd (**2**) model. These findings are supported by the values of the torsion angles reported in Table 4.

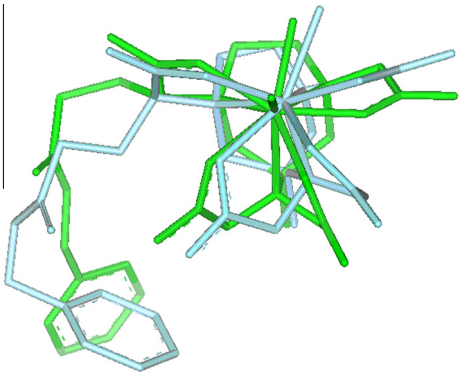

Fig. 6. Superimposition of the MD models of (αR,6R)-**L**-Gd (**1**, green) onto (αR,6S)-**L**-Gd (**2**, light blue) obtained through rms fitting of the heavy atoms. Hydrogen atoms are omitted for the sake of clarity. (For interpretation of the references to colour in this figure legend, the reader is referred to the web version of this article.)

Table 4
Selected torsion angles of the (**1**) crystallographic structure and the models of the two diastereoisomers resulting from MD calculation starting with one water coordinated.

Torsion angle (°)	X-ray (**1**)	Green (**1**)	Light blue (**2**)
O16–C18–C19–C20	−131	48	−53
N3–C13–C15–C16	156	162	178
O16–C17–C16–C15	−172	−63	92
C17–O16–C18–C19	−114	178	−69

The closer shift of the chelating atoms in the light blue structure of (**2**) towards the top of the polyhedron leads to the restriction of the solvent accessible surface close to the apical water, hindering the coordination of a further water molecule. Such a position could derive from an inward movement caused by the approaching of the phenyl ring to the coordination polyhedron. Thus, the light blue model (**2**) is a more compact molecule, able to coordinate only one water molecule in apical position, decreasing the likelihood of extracting water from the bulk.

4. Conclusions

The presence in AAZTA-C_2H_4COOBn of an extra moiety, beside introducing a stereocenter at C(13), gives also an additional carboxylic group with the potential for denticity, but the hindrance of the attached benzyl moiety disfavours metal coordination. The network of hydrogen bonds, related to the presence of four water molecules of which only one metal coordinated, is influenced by the extra moiety. In fact, the rather lipophilic substituent creates a kind of belt protecting the polymeric chains on one side and on the other forming lipophilic channels in the structure. The water molecules are interstitially located in the polymeric chains. The Molecular Dynamics results of the (αR,6S) isomer evidence the eight coordinated state of the Gd(III) ion, with the intervention of a metal coordinated water molecule, that is hydrogen bonded to three waters of the second coordination sphere, resembling the behaviour observed for the (αR,6R) isomer.

The structures analyzed by means of MD calculations show a different number of waters coordinated to the Gd(III) ion: the diastereoisomer (αR,6R)-**L**-Gd converged toward a structure having the Gd(III) ion nona-coordinated (two waters of coordination), while the (αR,6S)-**L**-Gd model remains octa-coordinated (one water of coordination). The geometry of the latter indicates that the lateral chain orientation as well as the stereochemistry of the chelating ligand could directly acting on the inner sphere coordination of the metal ion, preventing the water access to the Gd coordination sphere and affecting the relaxivity of the paramagnetic complex.

Appendix A. Supplementary material

Supplementary data associated with this article can be found, in the online version, at http://dx.doi.org/10.1016/j.ica.2013.08.004.

References

[1] P. Caravan, J.J. Ellison, T.J. McMurry, R.B. Lauffer, Chem. Rev. 99 (1999) 2293.
[2] A.E. Merbach, E. Toth, The Chemistry of Contrast Agents in Medical Magnetic Resonance Imaging, Wiley, Chichester, 2001.
[3] (a) P.H. Kuo, A. Abu-Alfa, R. Bucala, J. Griffith, K. Carlson, M. Girardi, J. Weinreb, S. Cowper, Appl. Radiology 38 (2009) 22–33;

(b) A. Kribben, O. Witzke, U. Hillen, J. Barkhausen, A.E. Daul, R. Erbel, J. Am. Coll. Radiol. 53 (2009) 1621–1628;
(c) S.K. Morcos, J. Haylor, World, J. Radiol. 2 (2010) 427–433.
[4] M. Port, J.-M. Idée, C. Medina, C. Robic, M. Sabatou, C. Corot, Biometals 21 (2008) 469.
[5] Z. Baranyai, Z. Palinkás, F. Uggeri, A. Maiocchi, S. Aime, E. Brücher, Chem. Eur. J. 18 (2012) 16426.
[6] J. Xu, S.J. Franklin, D.W. Whisenhunt Jr., K.N. Raymond, J. Am. Chem. Soc. 117 (1995) 7245.
[7] S. Hajela, M. Botta, S. Giraudo, J. Xu, K.N. Raymond, S. Aime, J. Am. Chem. Soc. 122 (2000) 11228.
[8] D.M.J. Doble, M. Botta, J. Wang, S. Aime, A. Barge, K.N. Raymond, J. Am. Chem. Soc. 123 (2001) 10758.
[9] P. Caravan, J.C. Amedio Jr., S.U. Dunham, M.T. Greenfield, N.J. Cloutier, S.A. McDermid, M. Spiller, S.G. Zech, R.J. Looby, A.M. Raitsimring, T.J. McMurry, R.B. Lauffer, Chem. Eur. J. 11 (2005) 5866.
[10] (a) J.B. Livramento, C. Weidensteiner, M.I.M. Prata, P.R. Allegrini, C.F.G.C. Geraldes, L. Helm, R. Kneuer, A.E. Merbach, A.C. Santos, P. Schmidt, Contrast Media Mol. Imaging 1 (2006) 30;
(b) J.B. Livramento, A. Sour, A. Borel, A.E. Merbach, Chem. Eur. J. 12 (2006) 989.
[11] S. Aime, L. Calabi, C. Cavallotti, E. Gianolio, G.B. Giovenzana, P. Losi, A. Maiocchi, G. Palmisano, M. Sisti, Inorg. Chem. 43 (2004) 7588.
[12] Z. Baranyai, F. Uggeri, G.B. Giovenzana, A. Bényei, E. Brücher, S. Aime, Chem. Eur. J. 15 (2009) 1696.
[13] S. Aime, G. Bombieri, C. Cavallotti, G.B. Giovenzana, D. Imperio, N. Marchini, Inorg. Chim. Acta 361 (2008) 1534.
[14] E. Gianolio, G.B. Giovenzana, D. Longo, I. Longo, I. Menegotto, Chem. Eur. J. 13 (2007) 5785.
[15] K.C. Briley-Saebo, S. Geninatti, A. Barazza, D. Cormode, W.J.M. Mulder, W. Chen, G.B. Giovenzana, S. Aime, Z.A. Fayad, J. Phys. Chem. B 113 (2009) 6283.
[16] S. Geninatti Crich, S. Lanzardo, D. Alberti, S. Belfiore, A. Ciampa, G.B. Giovenzana, C. Lovazzano, R. Pagliarin, S. Aime, Neoplasia 9 (2007) 1046.
[17] E. Gianolio, G.B. Giovenzana, A. Ciampa, S. Lanzardo, D. Imperio, S. Aime, ChemMedChem 3 (2008) 60.
[18] G. Gugliotta, M. Botta, G.B. Giovenzana, L. Tei, Bioorg. Med. Chem. Lett. 19 (2009) 3442.
[19] I. Mamedov, J. Engelmann, O. Eschenko, M. Beyerlein, N.K. Logothetis, Chem. Commun. 48 (2012) 2755.
[20] E. Gianolio, K. Ramalingam, B. Song, F. Kalman, S. Aime, R. Swenson, Inorg. Chem. Commun. 13 (2010) 663.
[21] G. Gugliotta, M. Botta, L. Tei, Org. Biomol. Chem. 8 (2010) 4569.
[22] L. Lattuada, A. Barge, G. Cravotto, G.B. Giovenzana, L. Tei, Chem. Soc. Rev. 40 (2011) 3019.
[23] E.M. Elemento, D. Parker, S. Aime, E. Gianolio, L. Lattuada, Org. Biomol. Chem. 7 (2009) 1120.
[24] K.-P. Eisenwiener, P. Powell, H.R. Mäcke, Bioorg. Med. Chem. Lett. 10 (2000) 2133.
[25] SIR-92, A. Altomare, M.C. Burla, M. Camalli, G. Cascarano, C. Giacovazzo, A. Gagliardi, G. Polidori, J. Appl. Crystallogr. 27 (1994) 435.
[26] G.M. Sheldrick, SHELXL97, Program for Refinement of Crystal Structure, University of Göttingen, Germany, 1997.
[27] U. Cosentino, A. Villa, D. Pitea, G. Moro, V. Barone, A. Maiocchi, J. Am. Chem. Soc. 12 (2002) 4901.
[28] M. Dolg, H. Stoll, A. Savin, H. Preuss, Theor. Chim. Acta 75 (1989) 173.
[29] M.J. Frisch, G.W. Trucks, H.B. Schlegel, G.E. Scuseria, M.A. Robb, J.R. Cheeseman, J.A. Montgomery Jr., T. Vreven, K.N. Kudin, J.C. Burant, J.M. Millam, S.S. Iyengar, J. Tomasi, V. Barone, B. Mennucci, M. Cossi, G. Scalmani, N. Rega, G.A. Petersson, H. Nakatsuji, M. Hada, M. Ehara, K. Toyota, R. Fukuda, J. Hasegawa, M. Ishida, T. Nakajima, Y. Honda, O. Kitao, H. Nakai, M. Klene, X. Li, J.E. Knox, H.P. Hratchian, J.B. Cross, V. Bakken, C. Adamo, J. Jaramillo, R. Gomperts, R.E. Stratmann, O. Yazyev, A.J. Austin, R. Cammi, C. Pomelli, J.W. Ochterski, P.Y. Ayala, K. Morokuma, G.A. Voth, P. Salvador, J.J. Dannenberg, V.G. Zakrzewski, S. Dapprich, A.D. Daniels, M.C. Strain, O. Farkas, D.K. Malick, A.D. Rabuck, K. Raghavachari, J.B. Foresman, J.V. Ortiz, Q. Cui, A.G. Baboul, S. Clifford, J. Cioslowski, B.B. Stefanov, G. Liu, A. Liashenko, P. Piskorz, I. Komaromi, R.L. Martin, D.J. Fox, T. Keith, M.A. Al-Laham, C.Y. Peng, A. Nanayakkara, M. Challacombe, P.M.W. Gill, B. Johnson, W. Chen, M.W. Wong, C. Gonzalez, J.A. Pople, GAUSSIAN 03 Revision C.02, Gaussian Inc., Wallingford CT, 2004.
[30] V. Barone, M. Cossi, J. Phys. Chem. A 102 (1998) 1995.
[31] H.J.C. Berendsen, J.R. Grigera, T.P. Straatsma, J. Phys. Chem. 91 (1987) 6269.
[32] J.C. Phillips, R. Braun, W. Wang, J. Gumbart, E. Tajkhorshid, E. Villa, C. Chipot, R.D. Skeel, L. Kale, K. Schulten, J. Comput. Chem. 26 (2005) 1781.
[33] H.J.C. Berendsen, J.P.M. Postma, W.F. van Gunsteren, A. Di Nola, J.R. Haak, J. Chem. Phys. 81 (1984) 3684.
[34] B. Hess, H. Bekker, H.J.C. Berendsen, J.G.E.M. Fraaije, J. Comput. Chem. 18 (1997) 1463.
[35] S. Miyamoto, P.A. Kollman, J. Comput. Chem. 13 (1992) 952.
[36] L.J. Farrugia, J. Appl. Crystallogr. 30 (1997) 565.
[37] G. Bombieri, N. Marchini, S. Ciattini, A. Mortillaro, S. Aime, Inorg. Chim. Acta 359 (2006) 3405.